Enhanced optoelectronic and thermoelectric activities of lead-free halide perovskite $NaGeCl_3$ under hydrostatic pressure

Student ID: 181317
Session: 2018-2019

Report submitted to the Department of Physics at
Jashore University of Science and Technology
in partial fulfillment of the requirements
for the degree of Bachelor of Science
with Honours in Physics

January 2024

Abstract

The full-potential linearized augmented plane wave (FP-LAPW) method based on density functional theory (DFT) is employed to investigate the structural, electronic, optical, and thermoelectric properties of $NaGeCl_3$ under various hydrostatic pressures, ranging from 0 to 8 GPa. At ambient pressure, the observed band gap is 1.17 eV, determined using the Tran-Blaha modified Becke-Johnson (TB-mBJ) potential. This material exhibits a direct $R \rightarrow R$ energy band gap, indicating semiconducting behavior at ambient pressure. The band gap decreases with increasing pressure, and at 8 GPa, the material transitions to a metallic state. Optical properties are explored by computing dielectric functions, reflectivity, optical conductivity, refractive index, absorption coefficient, extinction coefficient, and electron energy loss. Thermoelectric properties, calculated using the BoltzTraP code, include electrical conductivity, thermal conductivity, Seebeck coefficient, power factor, and figure of merit. Our findings suggest that the examined material holds potential for use in developing lead-free perovskite solar cells and other optoelectronic applications.

Acknowledgements

Firstly, I praise and thank almighty Allah, the Lord of the worlds, the most merciful, the guider of hearts, the provider of sustenance, the owner of life and death.

I would like to express gratitude to my respected supervisor, Dr. Mohammad Abdur Rashid for his continuous guidance and support that help me to complete my project work properly. I appreciate all the faculty members in the Department of Physics since they all contribute to our understanding of the subject and also thankful to my Quantum Materials Simulation Lab (QMSL) members who helped me directly or indirectly to learn things related to this project report. In addition, QMSL provided us many facilities, printing services is one of them.

Last but not least, I must never forget to thank my parents and brother for their effort, sacrifice and mental support to make me a better human.

Contents

List of Figures

List of Tables

Enhanced optoelectronic and thermoelectric activities of lead-free halide perovskite $NaGeCl_3$ under hydrostatic pressure

Chapter 1

Introduction

In the last decade, many researchers have been examining perovskite materials due to their potential applications in many industrial and technical fields such as photovoltaic, optoelectronic and thermoelectric devices [1–6]. Even though lead-containing compounds have demonstrated a lot of promise for photoluminescence applications [7], they are dangerous and toxic. The scientific community is focusing on alternative lead-free halide perovskites [8–13], leading to extensive investigations into their structural, electronic and optical properties. This detailed exploration aims to enhance our comprehension of the challenges associated with material applications.

The cubic perovskites general formula is ABX_3, where A and B is a cation and X is a anion. According to recent research, Ge-halide perovskites [6,14–16] offer remarkable qualities that make them ideal for a variety of uses, including solar cells. To analyze various physical properties of cubic perovskite, the first-principles calculations have been performed [17–20]. The application of external hydrostatic pressure is a simple and effective process that can modify the band gap of perovskites materials [20–29] which has an impact on the materials optical and electrical characteristics.

A lot of research has previously been done on the impact of hydrostatic pressure

on the physical properties of lead-free tin and germanium-based cubic halide perovskites $CsBX_3$(B = Sn, Ge; X= Cl, Br) [25–29]. Making lead-free, non-toxic halide perovskite is a fundamental issue in commercializing perovskite solar cells. In the visible energy range, Hassan et al. observed that the indirect band gap for $RbTaO_3$ widens and turns direct at 75 GPa, suggesting possible optoelectronic uses [30]. They observed that thermoelectric characteristics of $RbTaO_3$ at 0 and 75 GPa might potentially be applied in thermoelectric devices. According to Kholil et al, Fe-doped $CsSnCl_3$ shows higher potential for usage in solar cells and other photoelectric advancements [31]. Khan et al. reported that the perovskite compounds $RbSnCl_3$, $RbSnBr_3$, $KSnCl_3$, and $KSnBr_3$ have promising electrical and optical characteristics, suggesting their potential utilization in photovoltaic and other optoelectronic applications [32]. Md Borhanul Asfia et al. investigated pressure induced band gap shifting from ultra-violet to visible region of $RbSrCl_3$ perovskite [33]. They reported that at 150 GPa produced pressure, the band gap value of $RbSrCl_3$ drops to 2.09 eV, making it appropriate for use in optoelectronic devices. Mohammad Abdur Rashid et al. investigated the metallic behavior of semiconducting lead-free halide perovskites $RbSnX_3$ (X, Cl, Br) under pressure. They observed that these materials under pressure are more likely to be used in optoelectronic applications than zero pressure systems. Also, the optical functions suggest that the studied compound could be used in microelectronics, integrated circuits, OLEDs, QLEDs, waveguides, and surgical instruments. Furthermore, the optical properties indicate that the compound under study may find application in integrated circuits, waveguides, OLEDs, QLEDs, microelectronics, and surgical equipment [34]. In this work, we are inerested to investigate the structural, electronic, optical and thermoelectric properties of $NaGeCl_3$ for photovoltaic and optoelectronic applications.

This report is divided into five chapter. We begin with a brief introduction and motivation of the current work of investigated compound $NaGeCl_3$. We discuss in chapter 2 and 3 about the basic quantum mechanics and density functional theory respectively. In chapter 4, we explained observed result and calculation which is based on DFT. Finally in chapter 5 we present concluding summery of this work and also discuss about the potential application of our system.

Chapter 2

Basic quantum mechanics

2.1 Schrödinger equation

The Schrödinger equation is a linear partial differential equation that governs the wave function of a quantum-mechanical system. The time-independent single particle Schrödinger equation can be written as [35],

$$\hat{H}\psi(\vec{r}) = \hat{E}\psi(\vec{r}). \tag{2.1}$$

The Hamiltoninan for single particle is,

$$\hat{H} = \hat{T} + \hat{V} = -\frac{\hbar^2}{2m}\vec{\nabla}^2 + V(r). \tag{2.2}$$

This equation leads to the time independent single particle Schrödinger equation as,

$$\hat{E}\psi(\vec{r}) = \left[-\frac{\hbar^2}{2m}\vec{\nabla}^2 + V(\vec{r})\right]\psi(\vec{r}). \tag{2.3}$$

For N particles in three dimensions, the Hamiltonian is,

$$\hat{H} = \sum_{i=1}^{N} \frac{\hat{p}_i^2}{2m_i} + V(\vec{r}_1, \vec{r}_2, \ldots, \vec{r}_N). \tag{2.4}$$

Thus the time independent Schrödinger equation for N particle can be written as,

$$\hat{E}\psi(\vec{r}_1, \vec{r}_2, \ldots, \vec{r}_N) = \sum_{i=1}^{N} \frac{\hat{p}_i^2}{2m_i} + V(\vec{r}_1, \vec{r}_2, \ldots, \vec{r}_N)\psi(\vec{r}_1, \vec{r}_2, \ldots, \vec{r}_N). \tag{2.5}$$

2.2 The wave function

The first and most important postulates is that the state of a particle can be completely described by its (time-dependent) wave function. That means, it contains all information about the particle′s state. For the sake of simplicity, we will discuss the time indepedent wave. The physical interpretation for the square of the wave function as a probability density can be described by the Born probabilty interpretaion which is a major principle of the Copenhagen interpretation of quantum mechanics,

$$|\psi(\vec{r}_1, \vec{r}_2, \ldots, \vec{r}_N)|^2 d\vec{r}_1 d\vec{r}_2 \ldots d\vec{r}_N, \tag{2.6}$$

equation(2.6) describes the probability that particles $1, 2, ..., N$ are located simultaneously in the corresponding volume element $d\vec{r}_1 d\vec{r}_2 ... d\vec{r}_N$. But we should also consider for the case of two particle′s position are exchanged. The overall probability density can not depend on such an exchange, i.e.

$$|\psi(\vec{r}_1, \vec{r}_2, \ldots, \vec{r}_i, \vec{r}_j, \ldots, \vec{r}_N)|^2 = |\psi(\vec{r}_1, \vec{r}_2, \ldots, \vec{r}_j, \vec{r}_i, \ldots, \vec{r}_N)|^2. \tag{2.7}$$

When a particle is exchanged, then there will be only two possibilities for the behaviour of the wave function. As the first one is the symmetrical wave function, so it doesn′t change due to such an exchange. This corresponds (particles with integer or zero spin). Another possibility is an anti-symmetrical wave function, where an exchange of two particles causes a sign change, which corresponds to fermions (particles with half integer spin). The anti-symmetrical fermion wave function leads to the Pauli principle, which states that no two electrons can occupy the same state, whereas states means orbital and spin parts of the wave function [36]. The antisymmetry principle can be seen as the quantum-mechanical formalization of Paulie′s

theoretical ideas in the description of spectra [37]. For the probability interpretation, another consequence is the normalization of the wave function. If equation(2.8) describes the probability of finding a particle in a volume element, then result will gives as the probability of one, i.e. all particles must be found somewhere in space.

The normalization condition for the wave function is,

$$\int d\vec{r}_1 \int d\vec{r}_2 \ldots \int d\vec{r}_N |\psi(\vec{r}_1, \vec{r}_2, \ldots, \vec{r}_N)|^2 = 1 \tag{2.8}$$

For physical acceptable purpose, this condition is required. The wave functions must be continuous over the full spatial range and squar integrable [38]. By calculating the expectation values of operators with a wave functions, it provides the expectation value of the corresponding observable for the wave function [39]. For an observable $O(\vec{r}_1, \vec{r}_2, \ldots, \vec{r}_N)$,

$$O = \langle O \rangle = \int d\vec{r}_1 \int d\vec{r}_2 \ldots \int d\vec{r}_N \psi^*(\vec{r}_1, \vec{r}_2, \ldots, \vec{r}_N) \hat{O} \psi(\vec{r}_1, \vec{r}_2, \ldots, \vec{r}_N). \tag{2.9}$$

2.3 Born-Oppenheimer (BO)approximation

The Hamiltonian of a many body system consisting of nuclei and electrons can be written as,

$$\begin{aligned} H_{tot} = &- \sum_I \frac{\hbar^2}{2M_I} \nabla^2_{\boldsymbol{R}_I} - \sum_i \frac{\hbar^2}{2m_e} \nabla^2_{\boldsymbol{r}_i} + \frac{1}{2} \sum_{\substack{I,J \\ I \neq J}} \frac{Z_I Z_J e^2}{|\boldsymbol{R}_I - \mathbf{R}_J|} \\ &+ \frac{1}{2} \sum_{\substack{i,j \\ i \neq j}} \frac{e^2}{|\boldsymbol{r}_i - \boldsymbol{r}_j|} - \sum_{I,i} \frac{Z_I e^2}{|\boldsymbol{R}_I - \boldsymbol{r}_i|}. \end{aligned} \tag{2.10}$$

where the indexes I,J run on nuclei i and j on electrons, $\mathbf{R}_J$ and M_J and positions and masses of nuclei, $\mathbf{r}_i$ and m_e of the electrons, Z_i the atomic number of nucleus I. The first term is the kinetic energy of the nuclei, the second term is the kinetic energy of the electrons, the third term is the potential energy of nucleus-nucleus Coulomb interaction, the fourth term is the potential energy of electron-electron Coulomb

interaction and the last term is the potential energy of nucleus-electron Coulomb interaction. The time independent Schrödinger equation for the many-body system,

$$H_{tot}\psi(\{\mathbf{R}_I\},\{\mathbf{r}_i\}) = E\psi(\{\mathbf{R}_I\},\{\mathbf{r}_i\}). \tag{2.11}$$

where, $\psi(\{\mathbf{R}_I\},\{\mathbf{r}_i\})$ is the total wavefunction of the system.
In principle, everything about the system is known if one can solve the above Schrödinger equation. But in practice it is impossible. A so-called Born-Oppenheimer (BO) approximation was made by Born and Oppenheimer [40] in 1927. As the nuclei are much heavier than electrons, so the nuclei move much slower than the electrons. Therefore, we can separate the movement of nuclei and electrons. Therefore we can separate the movement of nuclei and electrons.

With the Born-Oppenheimer approximation equation(2.14)can be divided into two separate Schrödinger equations:

$$\begin{aligned} H_e = -\sum_i \frac{\hbar^2}{2M_e}\nabla^2_{\mathbf{r}_i} + \frac{1}{2}\sum_{\substack{I,J \\ I\neq J}} \frac{Z_I Z_J e^2}{|\mathbf{R}_I - \mathbf{R}_J|} + \frac{1}{2}\sum_{\substack{i,j \\ i\neq j}} \frac{e^2}{|\mathbf{r}_i - \mathbf{r}_j|} \\ - \sum_{I,i} \frac{Z_I e^2}{|\mathbf{R}_I - \mathbf{r}_i|}, \end{aligned} \tag{2.12}$$

and

$$[-\sum_I \frac{\hbar^2}{2M_I}\nabla^2_{\mathbf{R}I} + V(\{\mathbf{R}_I\})]\theta(\{\mathbf{R}_I\}) = E'\theta(\{\mathbf{R}_i\}). \tag{2.13}$$

The significance of the BO approximation is to separate the movement of electrons and nuclei. The electrons are moving in a static external potential $V_{ext}(\mathbf{r})$ formed by the nuclei which is the starting point of DFT.

2.4 The Hartree-Fock approach

In the spirit of the Born-Oppenheimer approximation, the electronic equation for molecules that depends parametically on the nuclear co-ordinates, is approximated using the Hartree-Fock method [41]. Hartree-Fock method is the method of approx-

imation for the determination of the wave function and the energy of a quantum many body system in a Schr"ødinger equation. Suppose that, ψ is approximated as an antisymmetrized product of N orthonormal spin orbitals $\psi_i(\vec{r})$, each a product of a spatial orbitals $\phi_k(\vec{r})$ and a spin function $\sigma(s) = \alpha(s)$ or $\beta(s)$, the Slater determinant,

$$\begin{aligned}\phi_{HF} &= \frac{1}{\sqrt{N!}}\begin{vmatrix} \psi_1(\vec{x}_1) & \psi_2(\vec{x}_1) & \cdots & \psi_N(\vec{x}_1) \\ \psi_1(\vec{x}_2) & \psi_2(\vec{x}_2) & \cdots & \psi_N(\vec{x}_2) \\ \vdots & \vdots & \ddots & \vdots \\ \psi_1(\vec{x}_N) & \psi_2(\vec{x}_N) & \cdots & \psi_N(\vec{x}_N) \end{vmatrix} \\ &= \frac{1}{\sqrt{N!}} det[\psi_1\psi_2\cdots\psi_N].\end{aligned} \tag{2.14}$$

A general expression for the Hartree-Fock energy is obtained by uses of the Slater determinant.

$$\langle\psi_{HF}|\hat{H}|\psi_{HF}\rangle = E_{HF} \tag{2.15}$$

$$(\sum_{i=1}^{N} H_i + \frac{1}{2}\sum_{i,j}^{N} J_{ij} - K_{ij})\psi_{HF} = E_{HF}\psi_{HF}, \tag{2.16}$$

where, the first term corresponds to the kinetic energy and the nucleus-electron interactions. So, the single particle contribution of the Hamiltonian is written as,

$$H_i = \int \psi^*(\vec{x})d\vec{x}[-\frac{1}{2}\nabla^2 + V(\vec{x}]\psi_i(\vec{x})d\vec{x}. \tag{2.17}$$

And the last term of equation(2.16) correspond to electron-electron interactions. They are called Coulomb (J_{ij}) and exchange integral (K_{ij}). We can write this term in the following way,

$$J_{ij} = \int\int \psi_i(\vec{x}_1)\psi_j^*(\vec{x}_1)\frac{1}{r_{12}}\psi_j^*(\vec{x}_2)\psi_j(\vec{x}_2)d\vec{x}_1 d\vec{x}_2. \tag{2.18}$$

$$K_{ij} = \int\int \psi_i^*(\vec{x}_1)\psi_j(\vec{x}_1)\frac{1}{r_{12}}\psi_j(\vec{x}_2)\psi_j^*(\vec{x}_2)d\vec{x}_1 d\vec{x}_2. \tag{2.19}$$

These integrals are all real and $J_{ij} \geq K_{ij} \geq 0$.

2.4.1 Limitations and failings of the Hartree-Fock approach

Atoms as well as molecules can have an even or odd number of electrons. If the number of electrons is even and all of them are located in double occupied spatial orbitals, then ϕ_i is the compound in a single state and such systems are called closed-shell systems. Compounds with an odd number of electrons as well as compounds with single occupied orbitals, i.e. species with triplet or higher ground state, are called open-shell system respectively. These two types of systems correspond to two different approaches of the Hartree-Fock method. In the restricted HF-method (RHF), all electrons are considered to be paired in orbitals whereas in the unrestricted HF (UHF)- method this limitation is lifted totally. It is possible to describe open-shell systems with a RHF approach where only the single occupied orbitals are excluded which is then called a restricted open-shell HF (ROHF) which is an approach closer to reality but also more complex and therefore less popular than UHF [42].

The size of the investigated system can also be a limiting factor for calculations. Kohn states a number of $M = p^5$ with $3 \leq p \leq 10$ parameters for a result with sufficient accuracy in the investigation of the H_2 system [43]. For a system with N = 100 (active) electrons the number of parameters rises to,

$$M = p^{3N} = 3^{300} to 10^{300} \approx 10^{150} to 10^{300}. \tag{2.20}$$

Since many electron can not be described entirely by a single Slater determinant, the energy obtained by HF calculations is always larger than the exact ground state energy. The most accurate energy obtainable by HF-methods is called the Hartree-Fock-limit. The difference between E_{HF} and E_{exact} is called the correlation energy and can be denoted as [44],

$$E_{corr}^{HF} = E_{min} - E_{Hf}. \tag{2.21}$$

Despite the fact that E_{corr} is usually small against E_{min}, as in the example of a N_2

molecule where,

$$E_{corr}^{HF} = 14.9eV < 0.001 \cdot E_{min}, \tag{2.22}$$

it can have huge influence [45].

For instance, the experimental dissociation energy of the N_2 molecule is,

$$E_{diss} = 9.9eV < E_{corr}, \tag{2.23}$$

which corresponds to a large contribution of the correlation energy to relative energies such as reaction energies which are particular interest in quantum chemistry. The main contribution to the correlation energy arises from the mean field approximation used in the HF-method. That means one electron moves in the average field of the other ones, an approach which completely neglects the intrinsic correlation of the electron movements. For better understanding purpose, one may picture the repulsion of electrons at small distances which clearly cannot be covered by a mean-field approach like the Hartree-Fock-method [42].

Chapter 3

Density functional theory

3.1 The electron density

The electron density (for N electrons) as the basic variables of density functional theory is defined as,

$$n(\mathbf{r}) = N \sum_{s1} \int d\mathbf{x}_2 \ldots \int d\mathbf{x}_N \psi^*(\mathbf{x}_1, \mathbf{x}_2, \ldots, \mathbf{x}_N)\psi(\mathbf{x}_1, \mathbf{x}_2, \ldots, \mathbf{x}_N). \tag{3.1}$$

So the wave function is dependent on spin and spatial coordinates. The integral in the equation gives the probability that a particular electron with arbitrary spin found in the volume element $d\mathbf{r}_1$. As the electrons are indistinguishable, N times the integral gives the probability that any electron is found there. The other electrons represented by the wave-function $\psi(\mathbf{x}_1, \mathbf{x}_2, \ldots, \mathbf{x}_N)$ have arbitrary spin and spatial coordinates [42]. If the spin coordinates are neglected, the electron density can be expressed as measurable observable which is only dependent on spatial coordinate,

$$n(\mathbf{r}) = N \int d\mathbf{r}_2 \ldots \int d\mathbf{r}_N \psi^*(\mathbf{r}_1, \mathbf{r}_2, \ldots, \mathbf{r}_N)\psi(\mathbf{r}_1, \mathbf{r}_2, \ldots, \mathbf{r}_N). \tag{3.2}$$

The total number of electron can be obtained by integrating the electron density over the spatial variables,

$$N = \int d\mathbf{r} n(\mathbf{r}). \tag{3.3}$$

3.2 Thomas-Fermi-Dirac approximation

The predecessor to DFT was the Thomas-Fermi (TF) model proposed by Thomas and Fermi in 1927 [46,47]. In this method, they used the electron density $n(\mathbf{r})$ as the basic variable instead of wave-function. The total energy of a system is an external potential $V_{ext}(\mathbf{r})$ is written as a function of the electron density $n(\mathbf{r})$ as:

$$E_{TF}[n(\mathbf{r})] = A_1 \int n(\mathbf{r})^{\frac{5}{3}} d\mathbf{r} + \int n(\mathbf{r}) V_{ext}(\mathbf{r} d\mathbf{r}) + \frac{1}{2} \int \int \frac{n(\mathbf{r}) n(\mathbf{r}')}{|\mathbf{r} - \mathbf{r}'|} d\mathbf{r} d\mathbf{r}'. \tag{3.4}$$

Where, the first term is the kinetic energy of the non-interacting electrons in a homogeneous electron gas (HEG) with $A_1 = \frac{3}{10}(3\Pi^2)^{\frac{2}{3}}$ in atomic units. The kinetic energy density of a HEG is obtained by adding up of the free-electron energy state $\varepsilon_k = \frac{k^2}{2}$ up to the fermi wave vector $k_F = [3\pi^2 n(\vec{r})]^{\frac{1}{3}}$ as:

$$t_o[n(\mathbf{r})] = \frac{2}{(2\pi)^3} \int_0^{k_F} \frac{k^2}{2} 4\pi k^2 dk = A_1 n(\mathbf{r})^{\frac{5}{3}}. \tag{3.5}$$

The second term is the classical electrostatic energy of the nucleus-electron Coulomb interaction. The Third term is the classical electrostatic Hartree energy approximated by the classical Coulomb repulsion between electrons. In 1930, Dirac extended the Thomas-Fermi method by adding a local exchange term $A_2 \int n(\mathbf{r})^{\frac{4}{3}} d\mathbf{r}$ to equation(3.4) with $A_2 = -\frac{3}{4}(\frac{3}{\pi})^{\frac{1}{3}}$, which leads equation(3.5) to,

$$\begin{aligned} E_{TFD}[n(\mathbf{r})] = A_1 \int n(\mathbf{r})^{\frac{5}{3}} d\mathbf{r} + \int n(\mathbf{r}) V_{ext}(\mathbf{r}) d\mathbf{r} + \frac{1}{2} \int \int \frac{n(\mathbf{r}) n(\mathbf{r})'}{|\mathbf{r} - \mathbf{r}'|} d\mathbf{r} d\mathbf{r}' \\ + A_2 \int n(\mathbf{r})^{\frac{4}{3}} d\mathbf{r}. \end{aligned} \tag{3.6}$$

The ground state density and energy can be obtained by minimizing the Thomas-Fermi-Dirac equation(3.6) subject to conservation of the total number (N) of elec-

trons. Now using Lagrange multiplier, the solution can be found as,

$$\delta\{E_{TED}[n(\mathbf{r})] - \mu(\int n(\mathbf{r}) - N)\} = 0, \tag{3.7}$$

where, μ is a constant known as a lagrange multiplier, whose physical meaning is the chemical potential. The equation(3.7) leads to Thomas-Fermi-Dirac equation,

$$\frac{5}{3}A_1 n(\mathbf{r})^{\frac{2}{3}} + V_{ext}(\mathbf{r}) + \int\int \frac{n(\mathbf{r})n(\mathbf{r})'}{|\mathbf{r}-\mathbf{r}'|}d\mathbf{r}' + \frac{4}{3}A_2 n(\mathbf{r})^{\frac{1}{3}} - \mu = 0, \tag{3.8}$$

this can be solved directly to obtain the ground state density. Althogh it is not good enough to describe electrons in matter.

3.3 The Hohenberg-Kohn theorems

DFT was proven to be an exact theory of many-body systems by Hohenberg and Kohn in 1964 [48]. It applies not only to condensed-matter systems of electrons with fixed nuclei, but also more to any system of interacting particles in an external potential $V_{ext}(\mathbf{r})$. The theory is based upon two theorem.

3.3.1 The HK theorem 1

The ground state particle density $n(\mathbf{r})$ of a system of interacting particles in an external potential $V_{ext}(\mathbf{r})$ uniquely determines the external potential $V_{ext}(\mathbf{r})$, except for a constant. So, the ground state particle density determines the full Hamiltonian, except for a constant shift of the energy. In principle, all the states including ground and excited states of the many-body wave functions can be calculated. This means that the ground state particle density uniquely determines all properties of the system completely.

Proof of the HK theorem 1:

Here, we will only consider the ground state of the system is non-degenerate. Also, the system is valid for degenerate ground state. The proof is based on minimum energy principle. Suppose there are two different external potential $V_{ext}(\mathbf{r})$ and

$V_{ext}(\mathbf{r}')$ which differ by more than a constant and lead to the same ground state density $n_0(\mathbf{r})$, but different ground state wave function ψ and ψ' with $\hat{H}\psi = \hat{H}\psi'$. Then the expression,

$$\begin{aligned} E_0 &< \langle\psi'|\hat{H}|\psi'\rangle \\ &< \langle\psi'|\hat{H}'|\psi'\rangle + \langle\psi'|\hat{H} - \hat{H}'|\psi'\rangle \\ &< E_0' + \int n_0(r)[V_{ext}(\mathbf{r}) - V_{ext}'(\mathbf{r})]d\mathbf{r}, \end{aligned} \tag{3.9}$$

similarly,

$$\begin{aligned} E_0' &< \langle\psi|\hat{H}'|\psi\rangle \\ &< \langle\psi|\hat{H}|\psi\rangle \ + \langle\psi|\hat{H}' - \hat{H}|\psi'\rangle \\ &< E_0 + \int n_0(r)[V_{ext}'(\mathbf{r}) - V_{ext}(\mathbf{r})]d\mathbf{r}. \end{aligned} \tag{3.10}$$

Adding equation(3.9) and (3.10) lead to the contradiction,

$$E_0' + E < E_0 + E_0'. \tag{3.11}$$

Hence, no two different external potentials $V_{ext}(\mathbf{r})$, can give rise to the same ground state density $n_0(\mathbf{r})$, i.e. the ground state density determines the external potential $V_{ext}(\mathbf{r})$, except for a constant.

3.3.2 The HK theorem 2

There exist an universal functional $F[n(\mathbf{r})]$ of the density, independent of external potential $V_{ext}(\mathbf{r})$, such that the global minimum value of the energy functional $E[n(\mathbf{r})] \equiv T[n(\mathbf{r})] + E_{int}[n(\mathbf{r})]$ is the exact ground state energy of the system and and the exact ground state density $n_0(\mathbf{r})$ minimizes the functional. Thus the exact ground state energy and density are fully determined by the functional $E[n(\mathbf{r})]$.

Proof of the HK theorem 2:

The universal functional $F[n(\mathbf{r})]$ can be written as,

$$F[n(\mathbf{r})] \equiv T[n(\mathbf{r})] + E_{int}[n(\mathbf{r})], \tag{3.12}$$

where, $T[n(\mathbf{r})]$ is the kinetic energy and $E_{int}[n(\mathbf{r})]$ is the interaction energy of the particles. According to variational principle, for any wave function ψ', the energy functional $E[\psi']$:

$$E[\psi'] = \langle\psi'|\hat{T} + \hat{V}_{int} + \hat{V}_{ext}|\psi'\rangle \tag{3.13}$$

has minimum value only when ψ' is the ground state wave function ψ_0, with the constraint that the total number of the particles is conserved. According to HK theorem 1, ψ' must correspond to a ground state with particle functional of $n'(\mathbf{r})$ and external potential $V'_{ext}(\mathbf{r})$, then $E[\psi']$ is a functional of $n'(\mathbf{r})$. According to variational principle:

$$\begin{aligned} E[\psi'] \equiv \langle\psi'|\hat{T} + \hat{V}_{int} + \hat{V}_{ext}|\psi'\rangle &= E[n'(\mathbf{r})] \\ &= \int n'(\mathbf{r})V'(\mathbf{r})d\mathbf{r} > E[\psi_0] \\ &= \int n_0(\mathbf{r})d\mathbf{r} + F[n_0(\mathbf{r}] \\ &= E[n_0\mathbf{r}]. \end{aligned} \tag{3.14}$$

Thus the energy functional $E[n(\mathbf{r})] \equiv \int n(\mathbf{r})V'_{ext}(\mathbf{r})d\mathbf{r} + F[n(\mathbf{r})]$ evaluated for the correct ground state density $n_0(\mathbf{r})$ is indeed lower than the value of this functional for any other density $n(\mathbf{r})$. Therefore by minimizing the total energy functional of the system with respect to variations in the density $n(\mathbf{r})$, one would find the exact ground state density and energy.

3.4 The Kohn-Sham (KS) equations

The Kohn-Sham approach is to replace the difficult interacting many-body system obeying the Hamiltonian equation(2.10) with a different auxiliary system that can be solved more easily. Since there is no unique prescription for choosing the simpler auxiliary system, this is an ansartz that rephrases the issues [49]. Kohn and Sham proposed that ground state density of the original interacting system is equal to that of some choosen noninteracting system. The most desirable way in which quantities can be calculated for problems without an exact analytical solution is one that allows iterations [39]. An early example of an iterative approach are the

self-consistent single particle Hartree equations. Hartree′s approximation assumes that every electron moves in an effective single-particle potential of the form,

$$\nu_H(\mathbf{r}) = -\frac{Z}{|\mathbf{r}|} + \int \frac{n(\mathbf{r})}{|(\mathbf{r}) - (\mathbf{r}')} d\mathbf{r}. \tag{3.15}$$

The first term is an attractive Coulomb potential of a nucleus with atomic number Z, whereas the intgral term corresponds to the potential caused by the mean electron density distribution $n(\mathbf{r})$. The mean density can be denoted in terms of the single particle wavefunctions,

$$n(\mathbf{r}) = \sum_{j=1}^{M} |\phi_j(\mathbf{r})|^2. \tag{3.16}$$

As electron-electron interactions are taken into account in the potential term, so the N-electron and 3-dimensional Schrödinger equation can be replaced by N 3-demensional single particle equations for electrons moving in an effective potential:

$$[-\frac{1}{2}\nabla^2 + \nu_H(\mathbf{r})]\phi_j(\mathbf{r}) = \epsilon_j \phi_j(\mathbf{r}). \tag{3.17}$$

To solve these self consistent Hartree-equation iteratively an electron density $n(\mathbf{r})$ and subsequently a potential $\nu_H(\mathbf{r})$ are defined, which is then used to solve equation (3.17) for the chosen wave function. Since the framework of Hohenberg and Kohn is formally exact, an extraction of the Hartree equations from their variational principle for the energy should provide even improvement and practically useful formulation of the second theorem [43]. So, kohn and Sham investigated the density functional theory applied to a system of N non-interacting electrons in an external potential, which is similar to Hartree′s approach.

Now, the expression for the energy of such a system is of the form,

$$E_{\nu(\mathbf{r})}[n'(\mathbf{r})] \equiv \int \nu(\mathbf{r})[n'(\mathbf{r})]d|\mathbf{r} + T_s[n'(\mathbf{r})] \geq E \tag{3.18}$$

where, $n'(\mathbf{r})$ ν-representable density for non-interacting electrons and $T_s[n'(\mathbf{r})]$ the kinetic energy of those non-interacting electrons [43]. Construction of Euler-Lagrange

equation for the non-interacting case equation(3.18) with density is,

$$\delta E_\nu[n'(\mathbf{r})] \equiv \int \delta n'(\mathbf{r})[\nu(\mathbf{r}) + \frac{\delta}{\delta n'(\mathbf{r})} T_s[n'(\mathbf{r})]|_{n'(\mathbf{r})=n(\mathbf{r})} - \epsilon] d\mathbf{r} = 0 \tag{3.19}$$

with $n'(\mathbf{r})$, the exact ground state density for the potential $\nu(\mathbf{r})$, and the Lagrangian multiplier ϵ to ensure particle density conservation. For a system of non-interacting electrons, the total ground state energy and particle density can be denoted as the sums,

$$E = \sum_{j=1}^{N} \epsilon_j \tag{3.20}$$

and

$$n(\mathbf{r}) = \sum_{j=1}^{N} |\phi_j(\mathbf{r})|^2 \tag{3.21}$$

Also, Kohn and Sham used the universal functional as an alternative formulation,

$$F[n'(\mathbf{r})] \equiv T_s[n'(\mathbf{r})] + \frac{1}{2} \int \frac{[n'(\mathbf{r})][n'(\mathbf{r})]}{|\mathbf{r} - \mathbf{r}'} d\mathbf{r} d\mathbf{r}' + E_{xc}[n'(\mathbf{r})]. \tag{3.22}$$

Here, $T_s[n'(\mathbf{r})]$ is the kinetic energy functional of non-interacting electrons and the second term is the Hartree term which describes the electrostatic self-repulsion of the electron density. The last term is the exchange-correlation term. Construction of Euler-Lagrange equations for the interacting case,

$$\delta E_\nu[n'(\mathbf{r})] \equiv \delta n'(\mathbf{r})[\nu_{eff}(\mathbf{r}) + \frac{\delta}{\delta n'(\mathbf{r})} T_s[n'(\mathbf{r})]|_{n'(\mathbf{r})=n(\mathbf{r})} - \epsilon] d\mathbf{r} = 0 \tag{3.23}$$

with

$$\nu_{eff}(\mathbf{r}) \equiv + \int \frac{[n(\mathbf{r})]}{|\mathbf{r} - \mathbf{r}'|} + \nu_x c(\mathbf{r}) \tag{3.24}$$

and functional derivative,

$$\nu_{xc}(\mathbf{r}) \equiv \frac{\delta}{\delta n'(\mathbf{r})} E_{xc}[n'(\mathbf{r})]|_{n'(\mathbf{r})=n(\mathbf{r})}. \tag{3.25}$$

Whereas the Euler-Lagrange equation resembles equation(3.18) up to the potential term. That′s why the minimizing density can be calculated in a way similar to the Hartree-approach described in equation(3.15) to (3.17). The corresponding

equations are the single-particle Schrödinger equation,

$$[-\frac{1}{2}\nabla^2 + \nu_{eff}(\mathbf{r})]\phi_j(\mathbf{r}) = \epsilon_j\phi_j(\mathbf{r}) \quad j = 1, \ldots, N \tag{3.26}$$

as well as the defining equation for the particle density,

$$n(\mathbf{r}) = \sum_{j=1}^{M} |\phi_j(\mathbf{r})|^2 \tag{3.27}$$

which form together with the effective potential $\nu_{eff}(\mathbf{r})$ in equation(3.24) the self-consistent Kohn-Sham Equation [43]. The accurate ground state energy can be expressed as,

$$E = \sum_j \epsilon_j + E_{xc}[n(\mathbf{r})] - \int \nu_{xc}(\mathbf{r})n(\mathbf{r})d\nu - \frac{1}{2}\int \frac{[n'(\mathbf{r})][n'(\mathbf{r})]}{|\mathbf{r} - \mathbf{r}'|}d\mathbf{r}d\mathbf{r}'. \tag{3.28}$$

This equation can be seen as the generalization of the energy expression obtained with the Hartree-approach.

Similar to the Hohenberg-Kohn theorems, also equation(3.26) to (3.28) are formally exact, that means if the exact $E_{xc}[n(\mathbf{r})]$ and $\nu_{xc}[n(\mathbf{r})]$ would be used, one would obtain the exact solution. Indeed Kohn-Sham approach has led to very useful approximations that are now the basis of most calculations that attepmt to make first principles or ab-initio prediction for the properties of condensed matter and large molecular systems [49].

Solving Procedure of Kohn-Sham equation:

Kohn and Sham proposed the practical approximation method of ion state in the monoelectron equation, which is the Kohn-Sham equation. So,

$$[-\frac{\hbar}{2m}\nabla^2 + V_{eff}(\mathbf{r})]\psi_i(\mathbf{r}) = \epsilon_{me}\psi_i(\mathbf{r})] \tag{3.29}$$

where, ϵ_{me} is the eigenvalue of the monoelectron equation, and V_{eff} is the effective

potential. The electron density $n(\mathbf{r})$ is described as,

$$n(\mathbf{r}) = \sum_{i=1}^{N} \psi_i^*(\mathbf{r})\psi_i(\mathbf{r}) \tag{3.30}$$

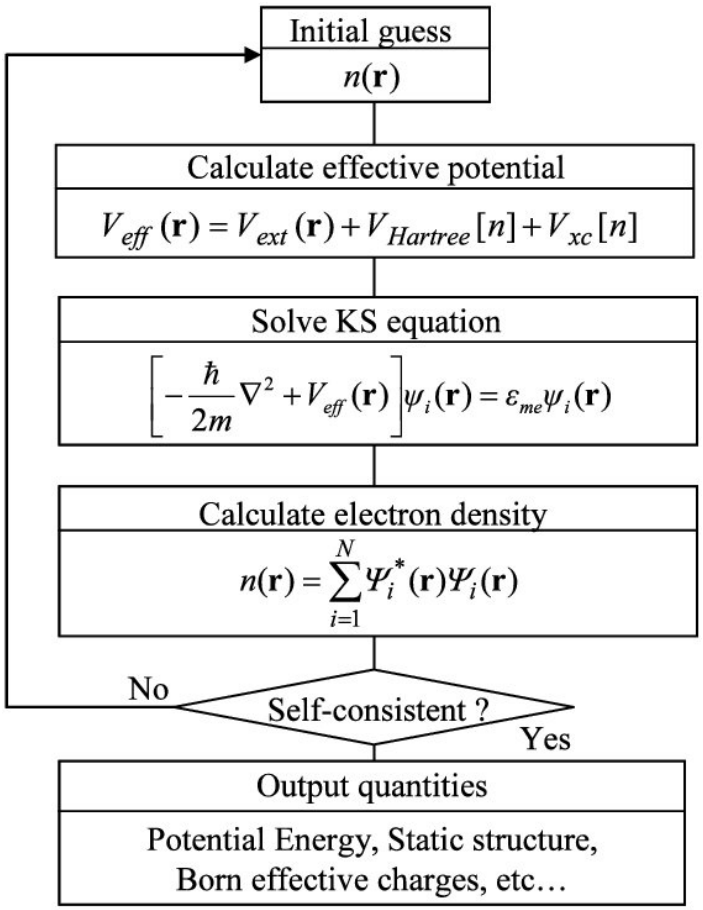

Figure 3.1: Flow chart of solving Kohn-Sham equation

Figure(3.1) shows the the solving of kohn-Sham equation. Firstly, the optional $n(\mathbf{r})$ is applied. By employing the approximation such as local density approximation (LDA) and the generalized gradient potential (GGA) for the exchange correlation potenial, the effective potential $V_{eff}(\mathbf{r})$ is estimated. And by using $V_{eff}(\mathbf{r})$ the wave-function $\psi(\mathbf{r})$ is determined. Then $\psi(\mathbf{r})$ is introduced into equation(3.30) to calculate the $n(\mathbf{r})$. This process is kept calculating until self-consistently converging [50].

In case of calculating the ion state of the solid such as a crystal, a unit cell structure is effectively adopted which is periodically arranged and have the wave function that

transfers with the real lattice vector $\mathbf{R}$, is described as,

$$\psi(\mathbf{r}) = \psi(\mathbf{r} + \mathbf{R}). \tag{3.31}$$

This wave function is described by using the wave vector $\mathbf{k}$.

$$\psi_j(\mathbf{r} + \mathbf{R}) = e^{i\mathbf{k}\mathbf{R}}\psi_j(\mathbf{r}). \tag{3.32}$$

This is called as the Bloch theorem. Applying Bloch theorem to the DFT, the potential energy of the unit crystal structure can be calculated under condition of periodic boundary.

3.5 Exchange-correlation (XC) functionals

The exchange-correlation potential of the Kohn-Sham density functional scheme is the difference between the Fermi potential an effective potential appearing in the one-electron Schrödinger equation for the square root of the electron density and the Pauli potential. But the major problem in solving the Kohn-Sham equations is that the true form of the exchange-correlation functional is not known. Two main approximation methods have been implemented to approximate the exchange-correlation functional. The simplest one known as the Local Density Approximations (LDA). It is based on knowledge of the energy of the infinte 3D homogeneous electron gas (HEG). For spin unpolarized system, the total exchange-correlation functional can be written as,

$$\begin{aligned} E_{XC}^{LDA}[n(\mathbf{r})] &= \int n(\mathbf{r})\epsilon_{XC}^{hom}(n(\mathbf{r}))d\mathbf{r} \\ &= \int n(\mathbf{r})[\epsilon_X^{hom}(n(\mathbf{r})) + \epsilon_C^{hom}(n(\mathbf{r}))]d\mathbf{r} \\ &= E_X^{LDA}[n(\mathbf{r})] + E_C^{LDA}[n(\mathbf{r})]. \end{aligned} \tag{3.33}$$

And for spin polarized system it will be,

$$E_{xc}^{LSDA}[n_\uparrow(\mathbf{r}), n_\downarrow(\mathbf{r})] = \int n(\mathbf{r})\epsilon_{xc}^{hom}(n_\uparrow(\mathbf{r}), n_\downarrow(\mathbf{r}))d\mathbf{r} \tag{3.34}$$

where, the Xc energy density $\epsilon_{XC}^{hom}(n(\mathbf{r}))$ is a function of the density, and it is decomposed into exchange energy density $\epsilon_{X}^{hom}(n(\mathbf{r}))$ and correlation energy density $\epsilon_{C}^{hom}(n(\mathbf{r}))$ so that the XC energy functional is decomposed into exchange energy functional $E_X^{LDA}(n(\mathbf{r}))$ and correlation functional $E_C^{LDA}(n(\mathbf{r}))$ linearly. The values of ϵ_{xc} were calculated by Ceperly and Alder using Quantum Monte Carlo techniques [51]. Although a gross approximation, LDA has been found to give good results in a wide range of solid state systems, but it neglects the inhomogeneities of the real charge density which is significantly different from the HEG result. This leads to development of generalised-gradient approximations (GGAs) which include density gradient corrections and higher spatial derivatives of the electron density and gives better results than LDA in many cases. Three most widely used GGAs are the forms proposed by Becke, Perdew et al. and Perdew, Burke and Enzerhof (PBE). The definition of the XC energy functional of GGA is the generalized form in equation(3.34) of LSDA to include corrections from density gradient $\nabla n(\mathbf{r})$ as,

$$\begin{aligned} E_{XC}^{GGA}[n_\uparrow(\mathbf{r}), n_\downarrow(\mathbf{r})] &= \int n(\mathbf{r})\epsilon_{XC}^{hom}(n_\uparrow(\mathbf{r}), n_\downarrow(\mathbf{r}), |\nabla n_\uparrow(\mathbf{r}), |\nabla n_\downarrow(\mathbf{r}), \ldots) d(\mathbf{r}) \\ &= \int n(\mathbf{r})\epsilon_{X}^{hom} F_{XC}(n_\uparrow(\mathbf{r}), n_\downarrow(\mathbf{r}), |\nabla n_\uparrow(\mathbf{r}), |\nabla n_\downarrow(\mathbf{r}), \ldots) d(\mathbf{r}), \end{aligned} \tag{3.35}$$

where, F_{XC} is dimensionless and $\epsilon_{XC}^{hom}(n(\mathbf{r}))$ is the exchange energy density of the unpolarized HEG. Although GGA do not offer a consistent improvement over LDA in all type of system, they have shown to improve on the LDA for calculations of molecular structures and in representing weak inter-molecular bonds [52]. The reason for the success of these approximations are not well understood, although this may be partially attributed to the fact that both obey the sum rule for the exchange-correlation hole in the electron density. The LDA and GGA give rise to a systematic overestimation of the electronic binding energy.

TB-mBJ: Local Density Approximation (LDA) is the first and most well-known approximation, which was followed by the Generalized Gradient Approximation (GGA) and further approximations. These potentials fail to reproduce the gap in semiconductors, but they do a fairly good job of reproducing the band structure of even complex metallic systems. A modification of the exchange and correla-

tion potential of Becke and Johnson (BJ) [53], the so-called Tran-Blaha modified Becke-Johnson (TB-MBJ) with LDA potential was published by Blaha et al. [54]. Compared to the previous available potentials, the new potential reproduces the experimental gaps by several orders of magnitude with greater accuracy. The modified TB-MBJ-LDA is,

$$V_{x,\sigma}^{MBJ}(r) = cV_{x,\sigma}^{BR}(r) + (3c-2)\frac{1}{\pi}\frac{\sqrt{5}}{12}\frac{\sqrt{2t_\sigma(r)}}{\rho_\sigma(r)}. \tag{3.36}$$

Where, $\rho_\sigma(r)$ is the density of states, $t_\sigma(r)$ is the kinetic energy density and $V_{x,\sigma}^{BR}(r)$ is the Becke-Roussel potential (BR) [55]. The c stands for,

$$c = \alpha + (\beta\frac{1}{V_{cell}}\int d^3r\frac{|\nabla\rho(r)|}{\rho(r)})^{\frac{1}{2}}, \tag{3.37}$$

where, α and β are free parameters.

Comparing the mBJ-LDA potential to the results from the previous version of the WIEN2k code, we find that it represents a significant improvement. Also For the theoretical analysis of complicated systems containing semiconductor compounds, such as surfaces, superlattices, and interfaces, this potential can be an invaluable tool.

Chapter 4

Result and discussion

4.1 Computational details

The full potential linearized augmented plane wave (FP-LAPW) method is the most accurate methods which are incorporated in the framework of WIEN2k code, which has been utilized for performing electronic structure calculations of crystals, which is based on the density functional theory [56]. Based on first principle calculation, the self-consistent schemes are utilized to investigate the electronic, optical characteristics of $NaGeCl_3$ structures. The WIEN2k package uses the LAPW method to calculate LSDA total energy, spin densities, Kohn-Sham eigenvalues at nuclear sites for a broad variety of space groups [57], which have a significant impact on the accuracy of the final result. We use Perdew Burke Ernzerhof - generalized gradient approximation (PBE-GGA) calculation to obtain optimized ground states of the material. PBE-GGA understimates the electronic band gap, while Tran-Blaha modified Becke-Johnson (TB-mBJ) with the local density approximation reproduces the band gap of semiconductors with improved accuracy in good agreement for the optical properties and band gap with experimental data. So, we calculate band structure, DOS, and optical properties by using exchange-correlation potential: TB-mBJ-LDA. The cut-off parameter $RK_{max} = 7.0$ is the maximum mutual lattice vector utilized

in plane wave dilation and R_{MT} is the smallest radius of muffin-tin sphere. The energy convergence criteria was set to 10^{-5} Ry, and the charge convergence criteria was set to $10^{-3}e$, where e is the charge of electron. Since a denser mesh of k-points is required to calculate the density of states and transport properties, we used $10 \times 10 \times 10$ k-points in the Brillouin zone (BZ), which is 1000 k-points in the total zone. Lastly, to examine the thermoelectric characteristics, Boltzmann theory is utilized and employing in BoltzTraP code at a temperature span from 100 K to 1000 K in the steps of 100 K.

4.2 Structural properties

The cubic $NaGeCl_3$ is the alkali halide perovskites that have the space group $Pm\bar{3}m$ (221). The unit cell structure of the perovskites is illustrated in Fig. 4.1(a), which is consists of five atoms (one formula unit). In the structure, the Na atom is located at $(0.0, 0.0, 0.0)$ Wyckoff position at the corner, the Ge atom is placed at $(0.5, 0.5, 0.5)$ Wyckoff position at the body center, and the Cl atom is residing at $(0.0, 0.5, 0.5)$ Wyckoff position at the face center. The WIEN2k software is used to visualize the optimized crystal structure.

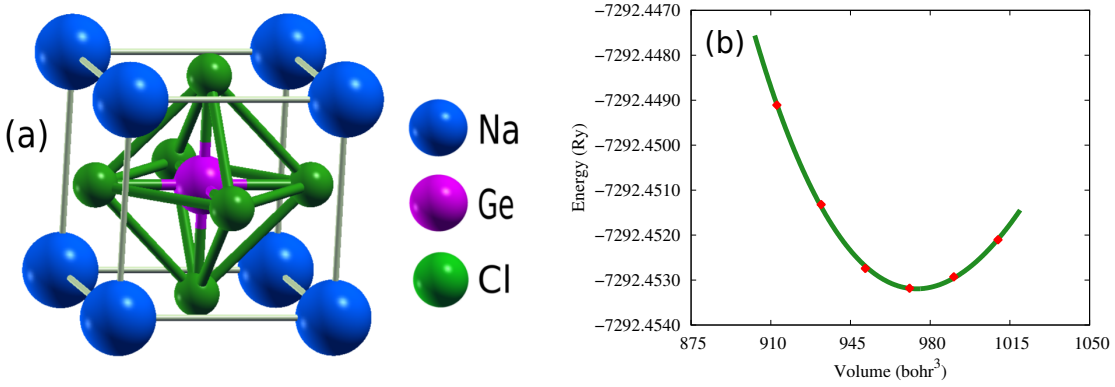

Figure 4.1: (a) Crystal Structure of $NaGeCl_3$ and (b) Total energy of $NaGeCl_3$ compound as a function of unit cell volume

We perform volume optimization to obtain lattice parameters of the ground state configuration minimum energy value of the system. The optimization energy vs unit cell volume of the compound is shown in Fig. 4.1(b), from which optimized lattice parameters are extracted by fitting the data to the Birch-Murnaghan equation

Table 4.1: The calculated lattice parameters (Å), Band gap of $NaGeCl_3$ at different hydrostatic pressure:

Pressures (GPa)	Lattice parameters (Å)	Band gap (eV)
0	5.25	1.17
2	5.14	0.73
4	5.06	0.38
6	5.00	0.15
8	4.95	0.00

of states [58]. These optimized lattice constants are then used to perform SCF calculation to investigate their electronic properties. The effects of the induced hydrostatic pressure on the lattice constant and band gap, are shown in Table 4.1. As the pressure rises, the lattice constant will drop, that means the distance between atoms decreases. Also induced pressure causes decreasing of band gap.

4.3 Electronic properties

The calculation of electronic properties of the investigated materials along with band structure and density of states provide useful data to understand it's optical properties. To compute DOS and band structure, we use mBJ potential which give an accurate band gap as compared to PBE approximation with experimental data. At 0 GPa pressure, the calculated band gap obtianed by using PBE-GGA approximation is 0.836 eV but it is 1.17 eV is obtained by using mBJ-LDA approximation. The electronic band structure, density of states and electron density are discussed in this section.

4.3.1 Band Structures

The investigation of the electronic band structure is necessary to understand the physical properties of crystalline solids which can provide information to describe optical properties. The estimated band structure of $NaGeCl_3$ under various pressure

are shown in Fig. 4.2. The black horizontal dashed line at 0 eV represents the Fermi level (E_f) which is set to zero and the valence band (VB) and conduction band (CB) are presented by colored lines below and above the E_F, respectively. Here, the calculation is done by defining highly symmetric points on the edge of the Brillouin zone with sampling path of $\Gamma - X - M - R - \Gamma - M$. At ambient pressure,

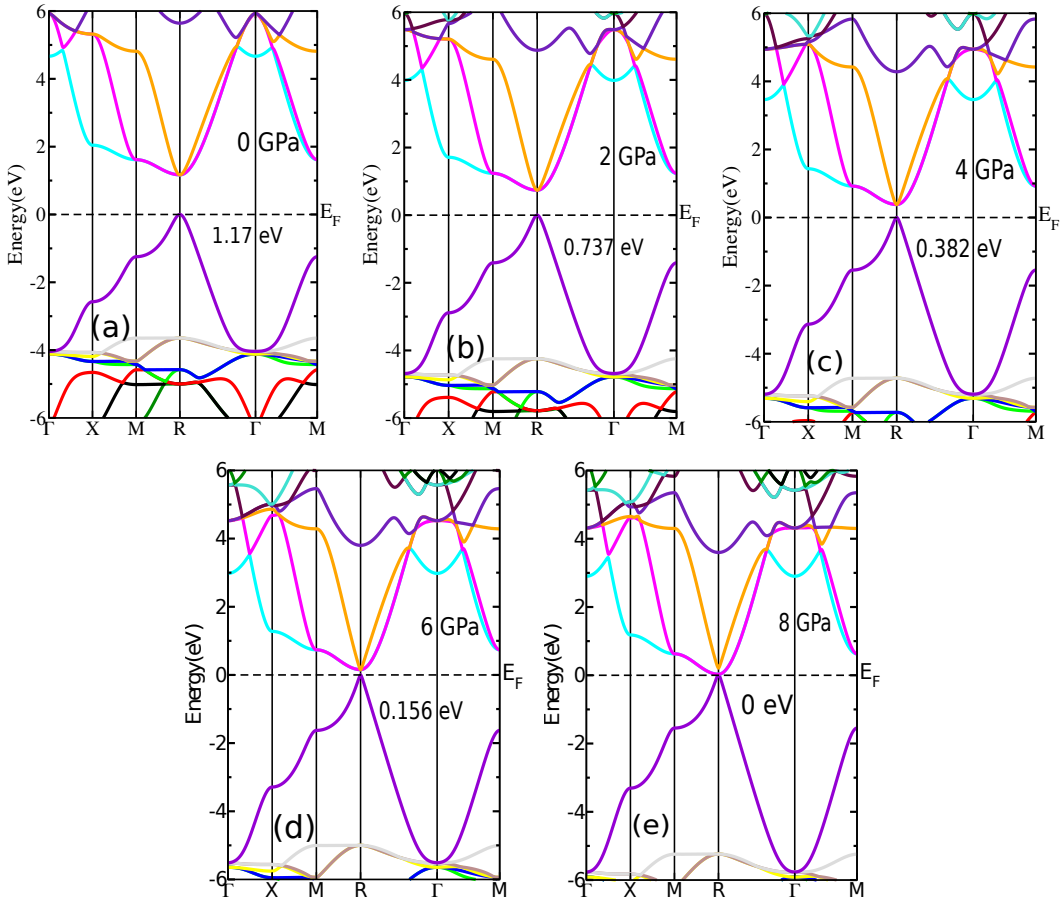

Figure 4.2: The calculated band Structures of $NaGeCl_3$ under various applied pressures

$NaGeCl_3$ has a direct band gap (E_g) of 1.17 eV at R point of the Brillouin zone. When pressure is increased, the conduction band minima at R point begin to move towards the E_F and it causes lowering of E_g. At 8 GPa pressure E_g vanishes, that means band gap reduced to zero because of inducing pressure and transforms from semiconducting to conducting nature.

4.3.2 Density of states

The density of states is the number of different states that electrons are permitted to occupy at a given energy level, i.e. the number of electron states per unit volume per unit energy. The total and partial DOS are calculated under various pressure to find the electronic characteristic of $NaGeCl_3$ which is shown in Fig. 4.3 by using mBJ level of theory. The black vertical dashed line at 0 eV represents E_F. Here,

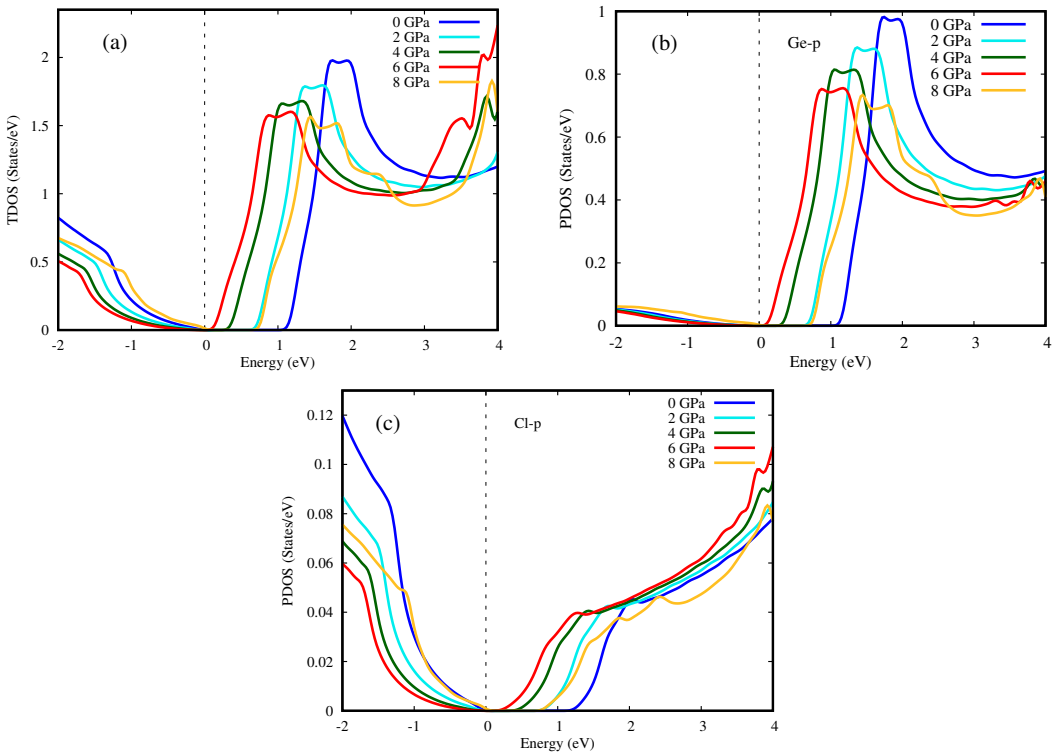

Figure 4.3: Total density of states (TDOS) and partial density of states (PDOS) of $NaGeCl_3$ under various applied pressure

at both non-pressurized and pressurized systems, the p-states of Cl atom dominate close to the top of the valence bands of the compounds. And near the bottom of the conduction band, the Ge-p orbital of the compounds makes the largest contribution to the total DOS of the perovskites. However, increasing of pressure reduces the contribution of Cl-p and Ge-p state. Furthermore, when pressure is incrementally applied this figure shows the feature of diminishing E_g.

4.3.3 Electron density

To investigate types of chemical bonds within the perovskites, the (100) and (101) charge density of cubic $NaGeCl_3$ under various applied pressure are plotted and presented in Fig. 4.4. Charge density is the measure of electric charge per unit area of a surface, or per unit volume of a body, which describes how much charge is stored in a particular field.

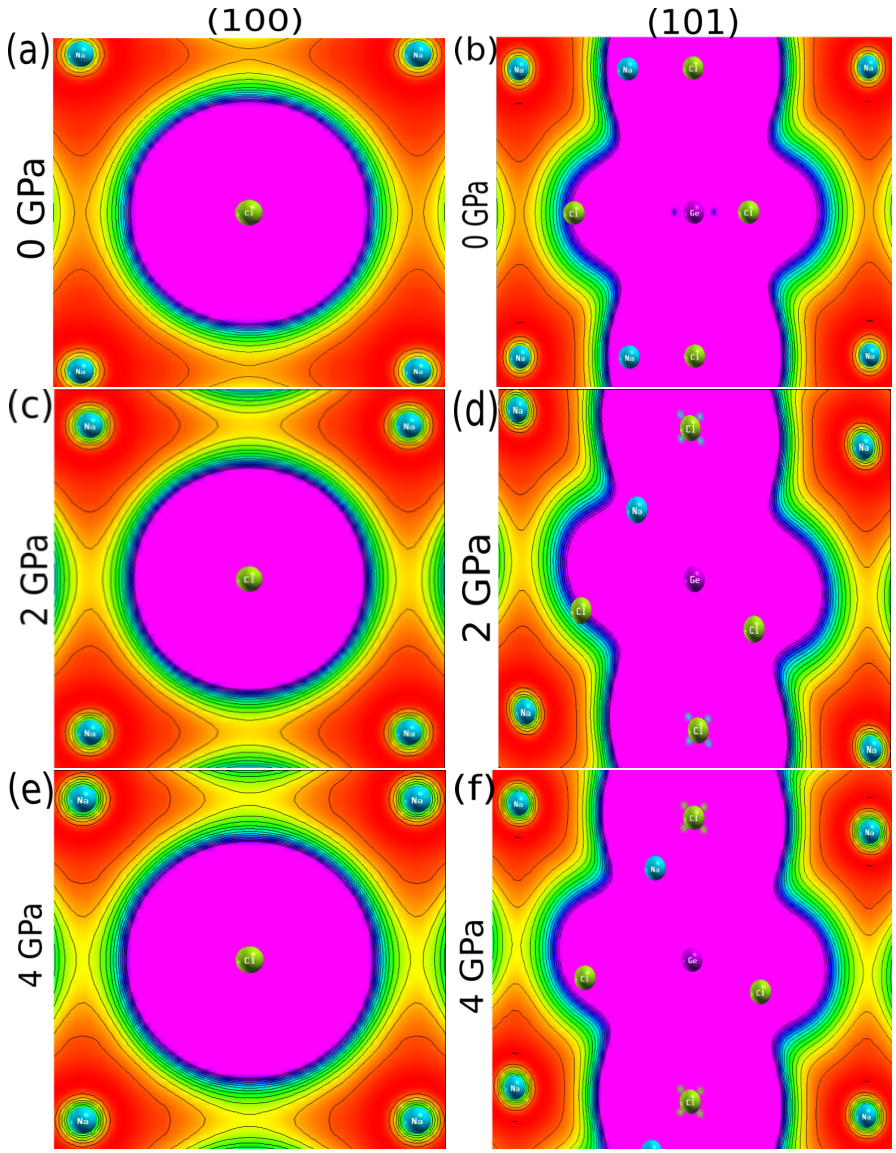

Figure 4.4: Electron density of (100) and (101) of $NaGeCl_3$ at 0, 2, 4 GPa pressure

At 0 GPa pressure, the charge distribution of Na and Cl atoms shows no overlap along (100) plane, showing ionic bonding between these two atoms and a overlapping

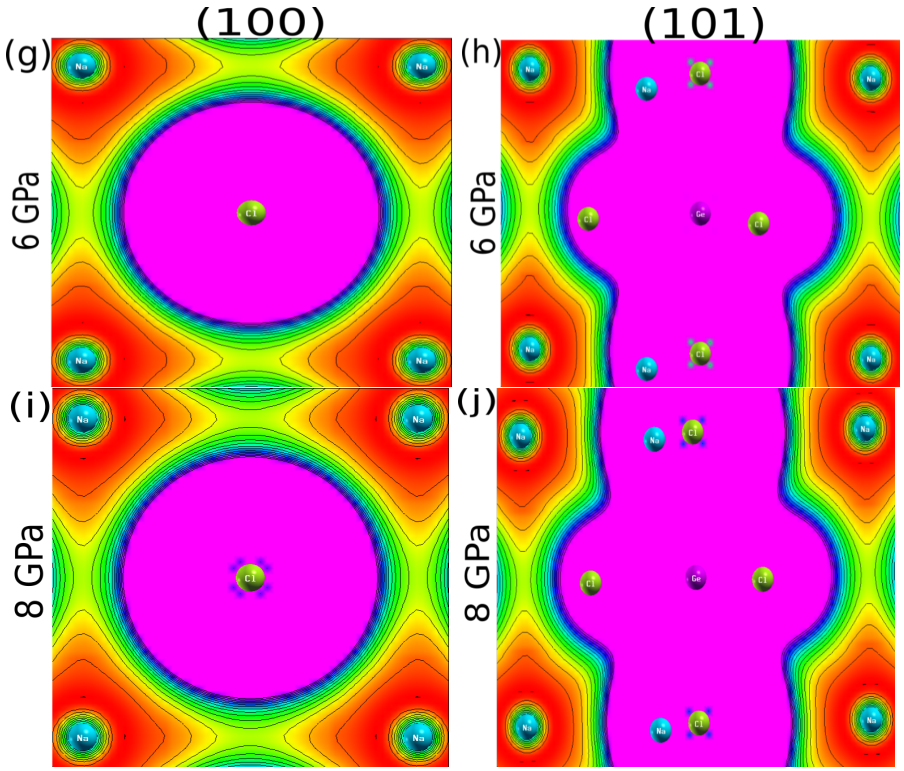

Figure 4.5: Electron density of (100) and (101) of $NaGeCl_3$ at 6 and 8 GPa pressure

characteristics can be seen between Ge and Cl atoms along (101) plane, revealing the covalent bonding. When pressure rises, the space between Na and Cl decreases along the (100) plane without overlapping the charge distribution, preserving the ionic character of Na-Cl bond. Also, overlapping between Ge and Cl atoms grows more along (101) plane as pressure increases, and it will strengthing the covalent nature of Ge-Cl bond.

4.4 Optical properties

To predict the performance of a material in optoelectronic device applications, optical functions should be understood. For that purpose, dielectric function, reflectivity, conductivity, refractive index, absorption coefficient, extinction coefficient and electron energy loss of $NaGeCl_3$ is investigated under various hydrostatic pressure. These properties are calculated by using TB-mBJ potential.

4.4.1 Dielectric function

The dielectric function demonstrates the dependency of a material's optical properties on incident wavelength of light and it can be given by written as,

$$\varepsilon(\omega) = \varepsilon_1(\omega) + i\varepsilon_2(\omega) \tag{4.1}$$

where, $\varepsilon_1(\omega)$ and $\varepsilon_2(\omega)$ are the real and imaginary components of the dielectric function respectively. The real part of dielectric function $\varepsilon_1(\omega)$ measures the polarization of incident photons, and the imaginary part of dielectric function $\varepsilon_2(\omega)$ measures the absorption of incident light photons by the material. The variation of $\varepsilon_1(\omega)$ and

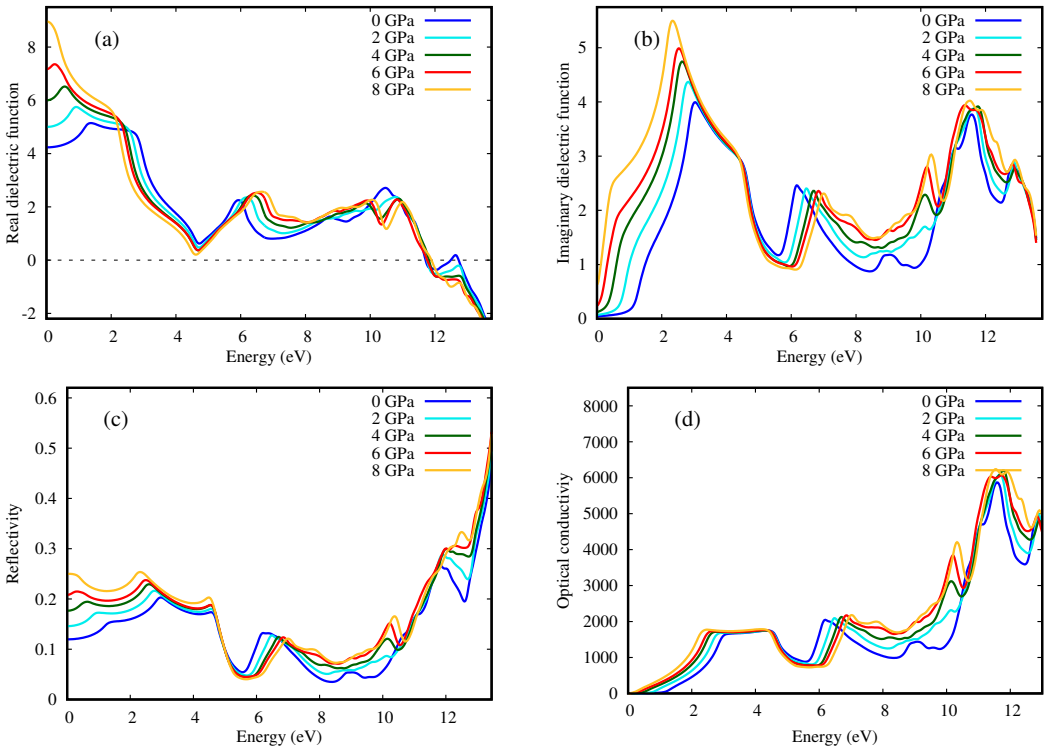

Figure 4.6: The pressure induced plot of (a) Real dielectric function $\varepsilon_1(\omega)$, (b) Imaginary dielectric function $\varepsilon_2(\omega)$, (c) Reflectivity, (d) Optical conductivity of $NaGeCl_3$ as a function of energy

$\varepsilon_2(\omega)$ with and without pressure are illustrated in Fig. 4.6 (a) and (b) respectively. The positive half is concerned with em wave propagation and the negative half is concerned with em wave absorption. So, the value of $\varepsilon_1(0)$ increases with the induced pressure which corresponds to the decrease in band gap and enhance device

efficiency. The energy absorption can be explained by $\varepsilon_2(\omega)$ which is related to the band structure and density of states of the material. As pressure rises, the peak value of $\varepsilon_2(\omega)$ also increases. Peaks represent charge carriers shifting from filled to empty bands. The $\varepsilon_2(\omega)$ decreases from a peak value with increase in energy.

4.4.2 Reflectivity and Optical conductivity

The optical reflectivity (R) is measured when light is incident on the surface of the material, which is used to detect the surface nature of a material, and it describes the potential of a surface to reflect light. The observed plot of reflectivity is presented in Fig. 4.6 (c). For energies exceeding 10 eV, the variation of reflectance under pressure is quite significant. The lower reflectivity in the energy region increases the potential of the metal halides to be used in optoelectronic devices.

Optical conductivity (σ) is a material property that describes the interaction between the induced current density in the material and the magnitude of the inducing electric field for arbitrarily elected frequencies. It identifies the electromagnetic response of a material. The graphical representation of optical conductivity as a function of energy is shown in Fig. 4.6 (d). Here, peaks get sharper with the application of hydrostatic pressure.

4.4.3 Refractive index and absorption coefficient

The refractive index (η) of a material gives information about how much path of light is bent when it enters that material. Fig. 4.7 (a) presents the plot of refractive index as a function of energy under various applied pressure and this feature is very similar to that of the real part of dielectric function $\varepsilon_1(\omega)$ (Fig. 4.6 (a)). It can be seen that at low energy limit, the refractive index has a high value.

The absorption coefficient (α) determines, how far into a material light with specific wavelength can penetrate before being absorbed. The material with large absorption coefficient have the ability to absorb the incident light rapidly. In Fig. 4.7 (b) the graphical representation of absorption coefficient as a function of energy

under various applied pressure is shown. The lowest energy for light absorption was about 0 to 1 eV. This strong absorption implies that the material can be used in optoelectronic applications.

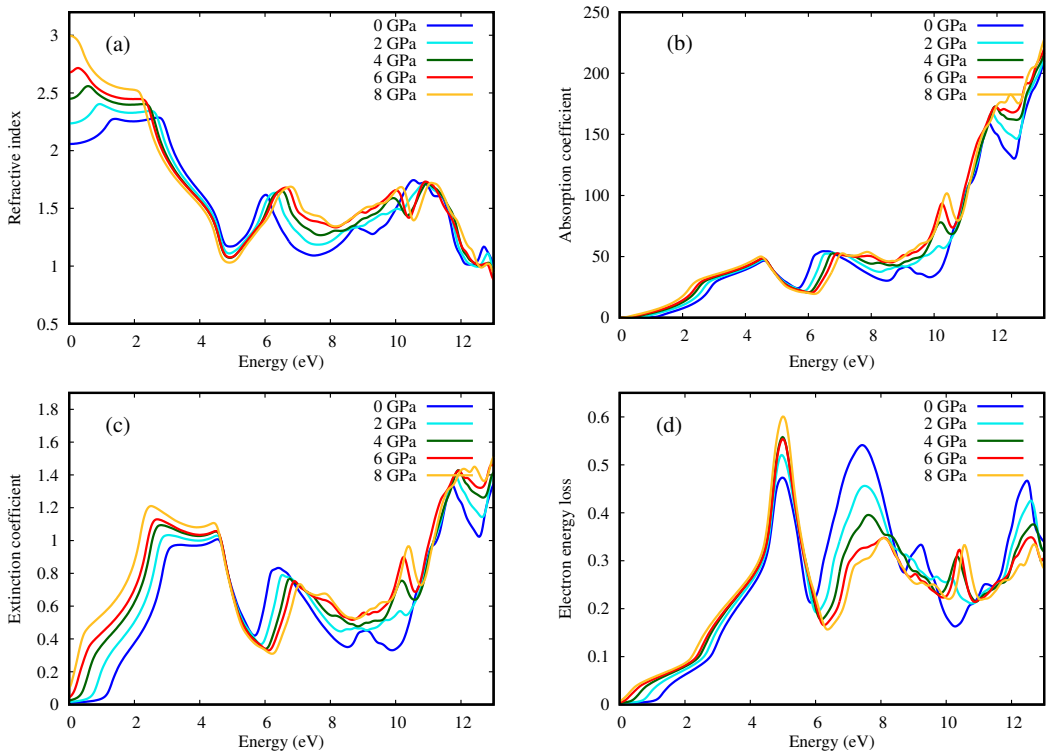

Figure 4.7: The pressure induced plot of (a) Refractive index, (b) Absorption coefficient, (c) Extinction coefficient, (d) Electron energy loss of $NaGeCl_3$ as a function of energy

4.4.4 Extinction coefficient and electron energy loss

The extinction coefficient is a characteristics that determines how strongly a species absorbs or reflects light at a particular wavelength. In Fig. 4.7 (c) Extinction coefficient vs energy curve is plotted at various induced pressure. It can be seen from here the extinction coefficient increases with the increasing of energy. The maximum value of extinction coefficient are found at high energy region.

In Fig. 4.7 (d), electron energy loss curve is plotted against energy under different hydrostatic pressure, where the loss is increased as the energy increases. The electron energy loss is an important factor which describes the energy loss of a fast moving electron in a material. In visible region absorption is small, so number of collisions

are small, hence electron energy loss is negligible. The opaqueness of the compounds is provide by high peak in electron energy loss after 4 eV. As the absoption increases beyond visible region, so due to increasing collision causes more electron energy loss.

4.5 Thermoelectric properties

To reduce environment pollution and to avoid energy disasters, thermoelectric material are of great inerest for transforming wasted heat into useful electricity. Thermoelectric parameters such as Seebeck coefficient (S), figure of merit (ZT), power factor ($\sigma S^2/\tau$), electrical conductivity (σ/τ) and thermal conductivity (κ_e/τ) are plotted against temperature under various hydrostatic pressure in Fig. 4.8. In evaluation of the transport characteristics, measurement of these parameters are required. The mobility of charge carriers is estimated in terms of the electric conductivity. The magnitude of electric conductivity is increased when pressure rises. Another part of conductivity comes from lattice vibration and thermal agitation, which is the thermal conductivity. The rate of increase in thermal conductivity is faster than the electrical conductivity. That means, at higher temperature more lattice vibrations are generated.

The potential difference induced by the temperature gradient is called the Seebeck coefficient.From figure we can see that, increasing temperature doesn′t affect largely to the seebeck coefficient. The power factor is another thermoelectric parameter that is used to determine the thermoelectric performance of any material. Power factor increases with an increase of temperature, which demonstrates suitability of this material for high temperature applications.

The thermoelectric performance (for power generation or cooling) depends on the efficiency of the thermoelectric material for transforming heat into electricity. The efficiency of a themoelectric material depends on the figure of merit $ZT = (S^2\sigma T/\kappa)$. For high efficiency, high electrical conductivity and low thermal conductivity is required. In Fig. 4.8 it can be seen that figure of merit curve increases with an increases of pressure at 2 and 4 GPa but suddenly decreases at 6 and 8 GPa. So

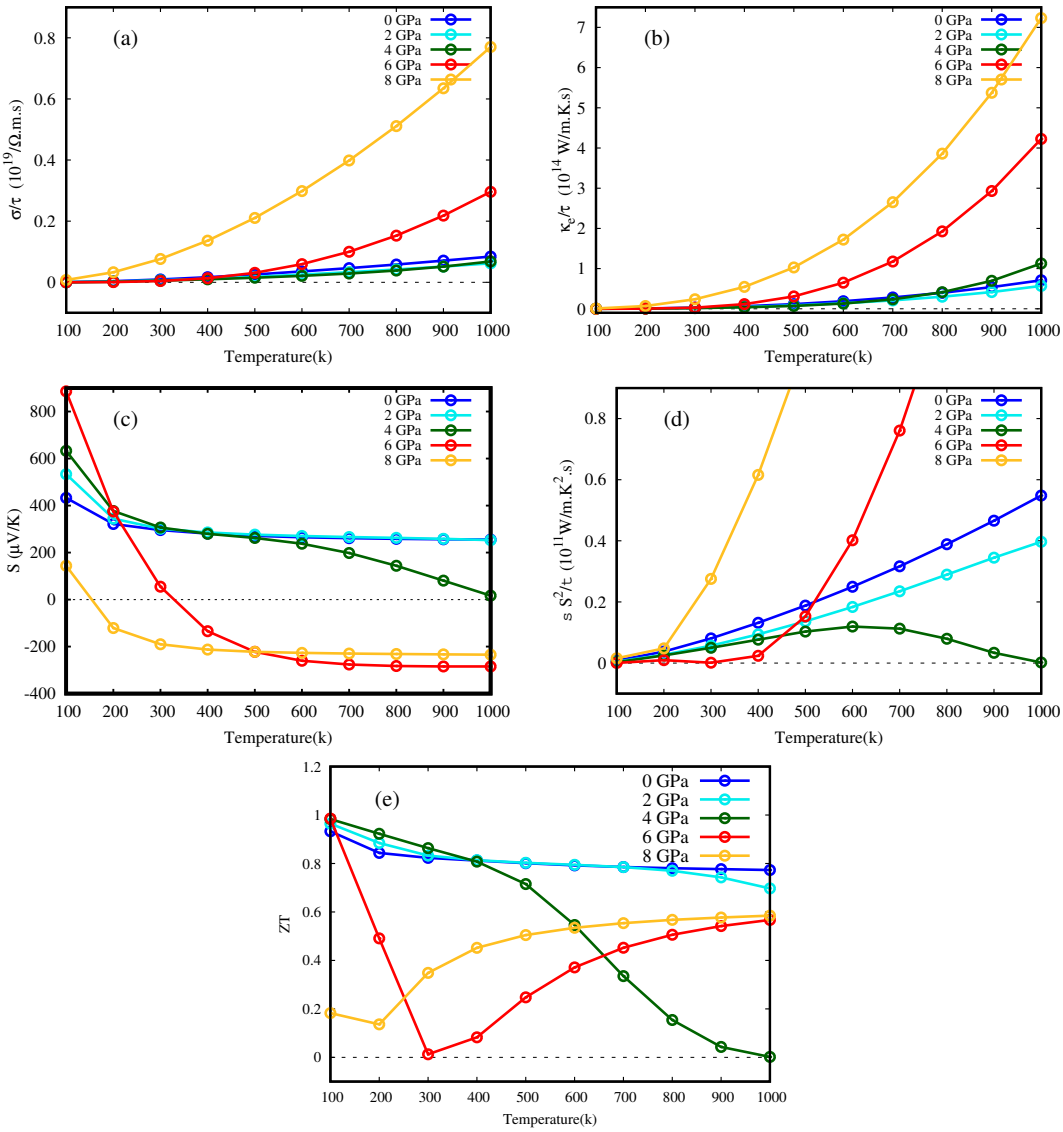

Figure 4.8: The pressure induced plot of (a) Electric conductivity, (b) Thermal conductivity, (c) Seebeck coefficient (d) Power factor, (e) Figure of merit of $NaGeCl_3$ as a funtion of temperature

working with below 6 GPa pressure will give good result. These observation indicates that this compositions have potential for use in thermoelectric applications.

Chapter 5

Conclusion

In this study, we investigated the structural, electronic, optical, and thermoelectric properties of the lead-free halide perovskite $NaGeCl_3$, utilizing the linearized augmented plane wave (LAPW) method based on density functional theory (DFT). Our findings reveal that $NaGeCl_3$ perovskite adopts a cubic structure with the space group $Pm\bar{3}m$ (221). The equilibrium lattice constant is determined to be 5.25 Å, obtained from the total energy versus unit cell volume plot for the ground state at zero pressure. At ambient pressure, the perovskite $NaGeCl_3$ exhibits a direct band gap of 1.17 eV, indicating its semiconducting nature. As pressure increases uniformly from 0 to 8 GPa, the direct band gap decreases from 1.17 to 0 eV, signifying a transition to metallic behavior under that pressure. Additionally, the optical properties demonstrate a significant absorption coefficient in the visible region, effectively tunable by hydrostatic pressure. The material also displays promising thermoelectric properties, characterized by good Seebeck coefficients and power factors. The obtained band gap value suggests the potential application of this material as an absorber for photovoltaic applications.

Bibliography

[1] Rasul Bakhsh Behram, M.A. Iqbal, S.M. Alay e Abbas, M. Sajjad, M. Yaseen, M. Imran Arshad, and G. Murtaza. Theoretical investigation of mechanical, optoelectronic and thermoelectric properties of $BiGaO_3$ and $BiInO_3$ compounds. *Mater. Sci. Semicon. Process.*, 41:297–303, 2016.

[2] N.A. Noor, Muhammad Rashid, S.M. Alay e Abbas, Mohsin Raza, Asif Mahmood, Shahid M. Ramay, and G. Murtaza. Shift of indirect to direct bandgap and thermoelectric response of the cubic $BiScO_3$ via DFT-mBJ studies. *Mater. Sci. Semicon. Process.*, 49:40–47, 2016.

[3] Mawloud Belabbas, Norredine Marbouh, Omar Arbouche, and Aamir Hussain. Optoelectronic properties of the novel perovskite materials $LiPb(Cl:Br:I)_3$ for enhanced hydrogen production by visible photo-catalytic activity: Theoretical prediction based on empirical formulae and DFT. *Int. J. Hydrogen Energy*, 45:33466–33477, 2020.

[4] Mehwish K. Butt, Muhammad Yaseen, Javed Iqbal, Abeer S. Altowyan, Adil Murtaza, Munawar Iqbal, and A. Laref. Structural, electronic, half –metallic ferromagnetic and optical properties of cubic $MAlO_3$ (M=Ce, Pr) perovskites: A DFT study. *J. Phys. Chem. Solid.*, 154:110084, 2021.

[5] Muhammad Yaseen, Haris Shafiq, Javed Iqbal, Misbah, Farwa Batool, Adil Murtaza, Munawar Iqbal, Hind Althib, Shahid M. Ramay, and Asif Mahmood. Pressure induced electronic, optical and thermoelectric properties of cubic $SrZrO_3$: DFT investigation. *Physica B: Condensed Matter*, 612:412626, 2021.

[6] Y. Selmani, H. Labrim, S. Ziti, and L. Bahmad. Electronic, optical and thermoelectric properties of the $CsMF_3$ (M= Si or Ge) fluoro-perovskites. *Comput. Condens. Matter*, 32:e00699, 2022.

[7] Riming Nie, Ranadeep Raj Sumukam, Sathy Harshavardhan Reddy, Murali Banavoth, and Sang Il Seok. Lead-free perovskite solar cells enabled by heterovalent substitutes. *Energy Environ. Sci.*, 13:2363–2385, 2020.

[8] Zhenyun Lan, Jie Meng, Kaibo Zheng, and Ivano E. Castelli. Exploring the intrinsic point defects in cesium copper halides. *J. Phys. Chem. C*, 125:1592–1598, 2021.

[9] Stephen J. Clark, Colin D. Flint, and John D. Donaldson. Luminescence and electrical conductivity of $CsSnBr_3$, and related phases. *J. Phys. Chem. Solids*, 42:133–135, 1981.

[10] J.C. Zheng, C.H.A. Huan, A.T.S. Wee, and M.H. Kuok. Electronic properties of $CsSnBr_3$: Studies by experiment and theory. *Surf. Interface Anal.*, 28:81–83, 1999.

[11] Ling-yi Huang and Walter R. L. Lambrecht. Electronic band structure, phonons, and exciton binding energies of halide perovskites $CsSnCl_3$, $CsSnBr_3$, and $CsSnI_3$. *Phys. Rev. B*, 88:165203, 2013.

[12] Mohammed Houari, B. Bouadjemi, Slimane Haid, Matougui Mohamed, Tayeb Lantri, Zoubir Aziz, Samir Bentata, and B. Bouhafs. Semiconductor behavior of halide perovskites $AGeX_3$ (A = K, Rb and Cs; X = F, Cl and Br): First-principles calculations. *Indian J. Phys.*, 94:455–467, 2019.

[13] M. I. Kholil, M. T. H. Bhuiyan, M. Atikur Rahman, M. S. Ali, and M. Aftabuzzaman. Influence of molybdenum and technetium doping on visible light absorption, optical and electronic properties of lead-free perovskite $CsSnBr_3$ for optoelectronic applications. *RSC. Adv.*, 11:2405–2414, 2021.

[14] Soukaina Bouhmaidi, Adil Marjaoui, Abdelali Talbi, Mohamed Zanouni, Kalid Nouneh, and Larbi Setti. A DFT study of electronic, optical and thermoelectric properties of Ge-halide perovskites $CsGeX_3$ (X=F, Cl and Br). *Comput. Condens. Matter*, 31:e00663, 2022.

[15] Y. Selmani, H. Labrim, M. Mouatassime, and L. Bahmad. Structural, optoelectronic and thermoelectric properties of Cs-based fluoroperovskites $CsMF_3$ (M= Ge, Sn or Pb). *Mater. Sci. Semicond.*, 152:107053, 2022.

[16] Sajid Khan, Nasir Mehmood, Rashid Ahmad, Asma Kalsoom, and Khalid Hameed. Analysis of structural, elastic and optoelectronic properties of indium-based halide perovskites $InACl_3$ (A = Ge, Sn, Pb) using density functional theory. *Mater. Sci. Semicond.*, 150:106973, 2022.

[17] Nguyen Hoang Linh, Nguyen Hoang Tuan, Dang Duc Dung, Phung Quoc Bao, Bach Thanh Cong, and Le Thi Hai Thanh. Alkali metal-substituted bismuth-based perovskite compounds: A DFT study. *J. Sci. Adv. Mater. Devices*, 4:492–498, 2019.

[18] Ismile Khan Shuvo, Md Saiduzzaman, Tariqul Islam Asif, Muhtasim Ali Haq, and Khandaker Monower Hossain. Shift of indirect to direct bandgap in going from K to Cs in $MCaF_3$ (M = K, Rb, Cs). *Solid State Sci.*, 16:152–157, 2013.

[19] N. Noor, M. Rashid, Syed Muhammad Alay-e Abbas, Mohsin Raza, Asif Mahmood, Shahid Ramay, and Ghulam Murtaza. Shift of indirect to direct bandgap and thermoelectric response of the cubic $BiScO_3$ via DFT-mBJ studies. *Mater. Sci. Semicond. Process*, 49:40–47, 2016.

[20] Abeeha Batool, M.A. Faridi, Q. Mahmood, Bakhtiar Ul Haq, A. Laref, and Saeed Ehsan Awan. The pressure-induced indirect to direct bandgap transition and thermoelectric response in $SrTiO_3$: An ab-initio study. *J. Phys. Chem. Solids*, 123:70–75, 2018.

[21] N. Noor, M. Rashid, Ghulam Mustafa, M.I. Khan, Asif Mahmood, and Shahid Ramay. Study of pressure induced physical properties of $ZnZrO_3$ perovskite using density functional theory. *Chem. Phys. Lett.*, 753:137601, 2020.

[22] Muhammad Yaseen, Mehwish Khalid Butt, Amna Ashfaq, Javed Iqbal, Maha M. Almoneef, Misbah, Munawar Iqbal, Adil Murtaza, and A. Laref. Phase transition and thermoelectric properties of cubic $KNbO_3$ under pressure: DFT approach. *J. Mater. Res. Technol.*, 11:2106–2113, 2021.

[23] Muhammad Yaseen, Haris Shafiq, Javed Iqbal, Misbah, Farwa Batool, Adil Murtaza, Munawar Iqbal, Hind Althib, Shahid M. Ramay, and Asif Mahmood. Pressure induced electronic, optical and thermoelectric properties of

cubic $SrZrO_3$: DFT investigation. *Phys. Rev. B Condens. Matter*, 612:412626, 2021.

[24] N.A. Noor, Q. Mahmood, M. Rashid, Bakhtiar Ul Haq, and A. Laref. The pressure-induced mechanical and optoelectronic behavior of cubic perovskite $PbSnO_3$ via ab-initio investigations. *Ceram Int.*, 44:13750–13756, 2018.

[25] Islam, J., Hossain, and A.K.M.A. Semiconducting to metallic transition with outstanding optoelectronic properties of $CsSnCl_3$ perovskite under pressure. *Sci. Rep.*, 10:14391, 2020.

[26] M.I. Kholil and M.T.H. Bhuiyan. Effects of pressure on narrowing the band gap, visible light absorption, and semi-metallic transition of lead-free perovskite $CsSnBr_3$ for optoelectronic applications. *J. Phys. Chem. Solids*, 154:110083, 2021.

[27] M. A. Islam, Md. Zahidur Rahaman, and Sapan Kumar Sen. A comparative study of hydrostatic pressure treated environmentally friendly perovskites $CsXBr_3$(X = Ge/Sn) for optoelectronic applications. *AIP Adv.*, 11, 2021.

[28] Md. Arif Islam, Jakiul Islam, Md Nazrul Islam, Sapan Sen, and A.K.M. Hossain. Enhanced ductility and optoelectronic properties of environment-friendly $CsGeCl_3$ under pressure. *AIP Adv.*, 11:45014, 2021.

[29] M.S. Hossain, M.M.H. Babu, T. Saha, M.S. Hossain, J. Podder, M.S. Rana, A. Barik, and P. Rani. Pressure induced semiconductor to metal phase transition in cubic $CsSnBr_3$ perovskite. *AIP Adv.*, 11:055024, 2021.

[30] Hassan M., Liaqat M., and Mahmood Q. Pressure dependence of electronic, optical and thermoelectric properties of $RbTaO_3$ perovskite. *Appl. Phys. A.*, 127:287, 2021.

[31] Md Kholil, Md. Tofajjol Bhuiyan, Md. Atikur Rahman, M. Ali, and Md Aftabuzzaman. Effects of Fe doping on the visible light absorption and bandgap tuning of lead-free ($CsSnCl_3$) and lead halide ($CsPbCl_3$) perovskites for optoelectronic applications. *AIP Adv.*, 11:035229, 2021.

[32] K. Khan, J. Sahariya, and A. Soni. Structural, electronic and optical modeling of perovskite solar materials $ASnX_3$ (A Rb, K; X Cl, Br): First principle investigations. *Mater. Chem. Phys.*, 262:124284, 2021.

[33] Md Borhanul Asfia, Sahadat Jaman, and Mohammad Abdur Rashid. Pressure induced band gap shifting from ultra-violet to visible region of $RbSrCl_3$ perovskite. *Mater. Res. Express*, 9:095902, 2022.

[34] Mohammad Abdur Rashid, Md Saiduzzaman, Arpon Biswas, and Khandaker Monower Hossain. First-principles calculations to explore the metallic behavior of semiconducting lead-free halide perovskites $RbSnX_3$ (X=Cl, Br) under pressure. *Eur. Phys. J. Plus*, 137:649, 2022.

[35] E. Schrödinger. An Undulatory Theory of the Mechanics of Atoms and Molecules. *Phys. Rev.*, 28:1049–1070, 1926.

[36] Arthur Jabs. Connecting spin and statistics in quantum mechanics. *Found. Phys.*, pages 776–792, 2010.

[37] W. PAULI. On the Connexion between the Completion of Electron Groups in an Atom with the Complex Structure of Spectra. *J. Phys.*, page 31:765, 1925.

[38] Nouredine Zettili. Quantum Mechanics: Concepts and Applications. 2009.

[39] Klaus Capelle. A bird's-eye view of density-functional theory. 2006.

[40] M. Born and R. Oppenheimer. Annalen der Physik. 1927.

[41] David J. Griffiths. Introduction to quantum mechanics. *Pearson Education*, 2, 2015.

[42] Prof. Dr. Wolfram Koch and Dr. Max C. Holthausen. A Chemist's Guide to Density Functional Theory. *Wiley-VCH*, 2001.

[43] W. Kohn. Nobel lecture: Electronic structure of matter wave functions and density functionals. *Rev. Mod. Phys.*, 71:1253–1266, 1999.

[44] Per-Olov Löwdin. Scaling problem, virial theorem, and connected relations in quantum mechanics. *J. Mol. Spectrosc.*, 3:46–66, 1959.

[45] M. Odelius and I. Josefsson. Quantum chemistry - lecture notes. 2009.

[46] Thomas LH. The calculation of atomic fields. *Math. Proc. Camb. Philos.*, pages 542–548, 1927.

[47] Elliott H Lieb and Barry Simon. The Thomas-Fermi theory of atoms, molecules and solids. *Adv. Math. (N Y)*, 23:22–116, 1977.

[48] P. Hohenberg and W. Kohn. Inhomogeneous Electron Gas. *Phys. Rev.*, 136:B864–B871, 1964.

[49] R.M. Martin. *Electronic Structure: Basic Theory and Practical Methods*. Cambridge University Press, 2004.

[50] Eiji Nakamachi, Hwisim Hwang, Yasutomo Uetsuji, and Hiroyuki Kuramae. Three-scale process-crystallographic analysis of a new biocompatible piezoelectric material $MgSiO_3$ generation. pages 206–210, 2010.

[51] J. P. Perdew and A. Zunger. Self interaction correction to density functional approximations for many electron systems. phys. *Phys. Rev. B*, 1981.

[52] Y.-M. Juan and E. Kaxiras. Application of gradient corrections to density functional theory of atoms and solids. *Phys. Rev. B*, pages 14944–14952, 1993.

[53] Axel D. Becke and Erin R. Johnson. A simple effective potential for exchange. *J. Chem. Phys.*, 124:221101, 2006.

[54] Fabien Tran and Peter Blaha. Accurate band gaps of semiconductors and insulators with a semilocal exchange-correlation potential. *Phys. Rev. Lett.*, 102:226401, 2009.

[55] A. D. Becke and M. R. Roussel. Exchange holes in inhomogeneous systems: A coordinate-space model. *Phys. Rev. A.*, 39:3761–3767, 1989.

[56] Peter Blaha, Karlheinz Schwarz, Georg K. H. Madsen, Dieter Kvasnicka, Joachim Luitz, Robert Laskowski, Fabien Tran, and Laurence D. Marks. WIEN2k an augmented plane wave plus local orbitals program for calculating crystal properties. page 1, 2018.

[57] P. Blaha, Karlheinz Schwarz, P. Sorantin, and S.B. Trickey. Blaha, p., schwarz, k., sorantin, p. trickey, s.b. Full-potential, linearized augmented plane wave programs for crystalline systems. *Comput. Phys. Commun.*, 59:399–415, 1990.

[58] Murnaghan FD. The Compressibility of Media under Extreme Pressures. *Proc. Natl. Acad. Sci. U. S. A.*, pages 244–247, 1944.